Element Selective X-Ray Detected Magnetic Resonance

J. Goulon*, A. Rogalev*, F. Wilhelm*, N. Jaouen*, C. Goulon-Ginet*, G. Goujon*, J. Ben Youssef† and M.V. Indenbom†

*European Synchrotron Radiation Facility (ESRF), B.P. 220, 38043 Grenoble Cedex, France
†Laboratoire de Magnétisme de Bretagne, CNRS FRE 2697, UFR Sciences et Techniques, 29328 Brest Cedex 03, France

Abstract. Element selective X-ray Detected Magnetic Resonance (XDMR) was measured on exciting the Fe K-edge and Y L-edges in a high quality Yttrium Iron Garnet (YIG) thin film. Resonant pumping at high microwave power was achieved in the nonlinear foldover regime and X-ray Magnetic Circular Dichroism (XMCD) was used to probe the time-invariant change of the magnetization ΔM_z due to the precession of the relevant magnetization components at the Fe or Y sites. This challenging experiment required us to design a specific instrumentation. Emphasis is to be laid on the pure *orbital* character of the effective operators responsible for a K-edge XMCD signal: the XDMR experiment measured at the Fe K-edge thus produces a direct evidence of the forced precession of *orbital* magnetization DOS.

Keywords: XDMR,XMCD,FMR
PACS: 75.25.+z, 76.50+g, 78.20.Ls, 78.47.+p

INTRODUCTION

X-ray Magnetic Circular Dichroism (XMCD) benefits of the unique advantage to be element/edge selective and became particularly attractive when magneto-optical sum-rules made it possible to resolve the contributions of spin and orbital moments at different sites [1]. We discuss below how XMCD can be used to probe *locally* the resonant precession of spin/orbital magnetization components under the influence of a strong microwave pump field [2]. X-ray Detected Magnetic Resonance (XDMR) is then a transposition into the X-ray regime of Optically Detected Magnetic Resonance (ODMR) [3]. An alternative approach to the same physics was explored by Bailey *et al.* who combined time-resolved soft X-ray reflectometry with Pulsed Induction Magnetometry (PIM) [4]. XDMR spectra recorded in the frequency domain, however, offer better prospects to extract very weak signals from noise whereas resonance frequencies up to the THz range could potentially be reached at the ESRF.

As shown in Figure 1, two different XDMR geometries can be envisaged. In the *longitudinal* geometry, the wavevector $\mathbf{k}_x$ of the incident, circularly polarized (cp) X-rays is nearly parallel to the static magnetic *bias* field $\mathbf{H}_0$ whereas the microwave pump field $\mathbf{h}_p$ oscillates in a direction perpendicular to $\mathbf{H}_0$. If one assumes that the length of the equilibrium magnetization (M_s) remains invariant in the precession, there should be along the direction of $\mathbf{H}_0$ a time-invariant change of the magnetization ΔM_z that could be probed by XMCD. In the *transverse* geometry, the wavevector $\mathbf{k}_x$ of the incident cp X-rays would be set perpendicular to both $\mathbf{H}_0$ and $\mathbf{h}_p$: what should now be measured is a stronger XMCD signal proportional to the transverse magnetization $\Delta M_\perp$ but oscillating at the microwave frequency. In both cases, the XMCD/XDMR signal is recorded in the X-ray fluorescence excitation mode.

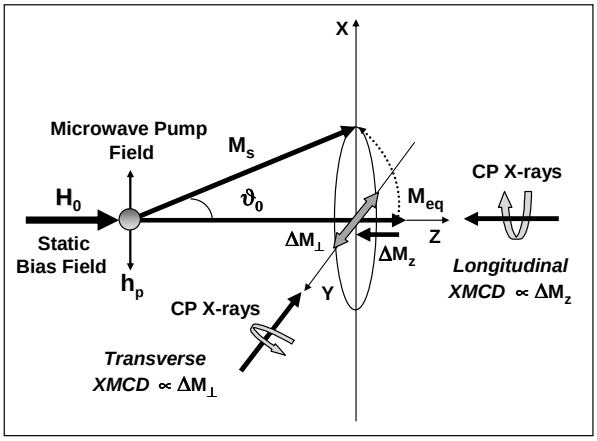

FIGURE 1. XDMR detection in *Longitudinal* and *Transverse* geometries. Note the time-invariant character of ΔM_z.

What makes the longitudinal geometry more attractive is the argument that no fast X-ray detector is required because the XDMR signal is proportional to the microwave power that can be amplitude modulated at low frequency. There is, nevertheless, a price to be paid: since the precession opening angle θ_0 is small, ΔM_z is only a 2nd order effect in comparison with $\Delta M_\perp$ and the signal is always very small. To enhance sensitivity, it is desirable to increase the microwave power at the expense of running into the nonlinear foldover regime of FMR [5]. Fortu-

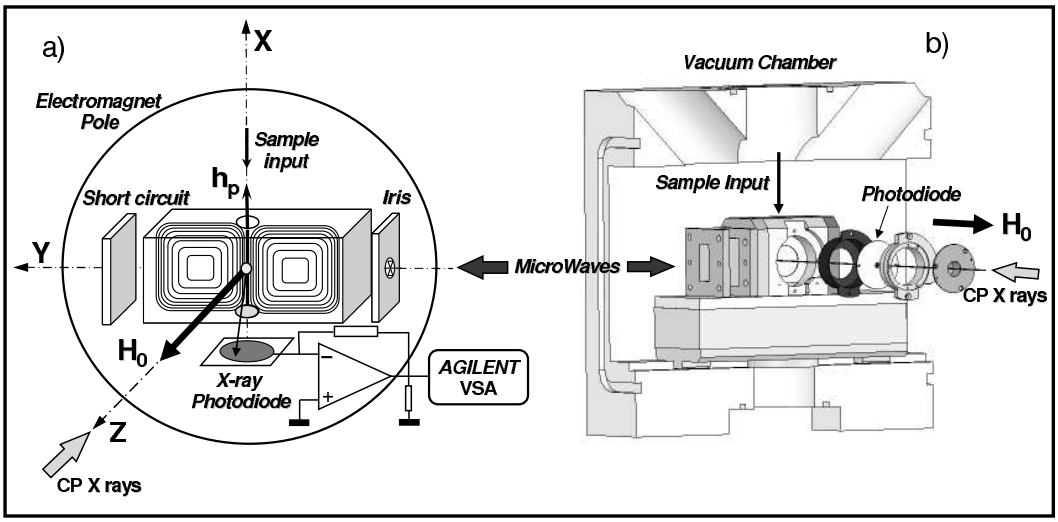

FIGURE 2. a) Field distribution in the TE_{102} rectangular cavity used for the 1rst XDMR experiments at the Fe K-edge. b) Configuration used for XDMR experiments at the Y L-edges. X-ray fluorescence photons are now collected in the backscattering geometry using a photodiode that has a 4 mm ⊘ hole at its center.

nately, it was recognized long time ago by Bloembergen and co-workers [6] that the longitudinal geometry was much less sensitive to magnon-magnon scattering processes and would offer a much higher saturation limit regarding the microwave pump power.

XDMR SPECTROMETER

A spectrometer has been built which allows us to record XDMR spectra at high microwave pumping power over the microwave frequency range 1-18 GHz. This instrument, which is now operational only in the longitudinal geometry, was designed to work as well in the transverse geometry, but only at low microwave frequencies. The ESRF XDMR spectrometer is permanently installed on beamline ID12 [7] which was optimized to record high quality XMCD spectra at the K-edges of all 3*d* transition metals as well as at the L-edges of the rare-earths and all 4*d*-5*d* transition elements. The X-ray sources are powerful helical undulators delivering high photon fluxes over the whole energy range 1.8-18 keV.

The arrangement of the X-band microwave bridge has been detailed elsewhere [8]. The microwave source is a wide-band generator with a very low phase noise (Anritsu MG-3692). Two amplification stages make it possible to handle a high microwave pumping power: (i) a low noise solid state amplifier (Miteq AMF-4B) can deliver up to 32 dBm; (ii) a microwave power module (Litton MPM-1020) based on a micro-TWT device can deliver up to 50 dBm. For the experiments which we report below on YIG thin films, the 2nd amplification stage was by-passed. A circulator (Channel Microwave Inc.) is used to extract the signal reflected back from the microwave cavity. This signal and a properly amplified component from the reference arm are fed together into a phase discriminator (Anaren 20758) in order to record high quality conventional FMR spectra. For XDMR experiments carried out in the longitudinal geometry, the microwave power is square-modulated using a fast switch (Miteq: SPST 124796) featuring over 80 dB isolation with a very short rise/fall time ($\leq$ 2 ns).

All experiments reported below were performed with the sample inserted into a home-made TE_{102} rectangular X-band cavity. The resonance frequency of the empty cavity was typically $F_{cav} \approx 9.450$ GHz with $Q_L \leq 4300$. The mechanical design of the cavity was optimized in order to maximize the solid angle over which the excited X-ray fluorescence photons can be collected.

The first XDMR experiment which we reported in reference [2], was carried out in the configuration sketched in Fig. 2a: the incident X-ray beam, propagating parallel to the magnetic bias field $\mathbf{H}_0$, entered the cavity through a small hole (⊘ 3 mm) drilled in the cavity in a place where the microwave electric field is minimum; two additional apertures (⊘ 9 mm) located at the top and bottom of the cavity made it possible to introduce the sample holder and to collect the X-ray fluorescence photons emitted along the direction of the microwave pump field h_p, *i.e.* at 90° from the incident X-ray beam. In order to minimize the X-ray fluorescence reabsorption, the sample could not be kept perpendicular to $\mathbf{H}_0$ and was inclined by an arbitrary tilt angle: $\beta_N = -30°$.

Recently, the sensitivity and the performances of the XDMR spectrometer were strongly enhanced using a new cavity in which the X-ray fluorescence photons can

be collected in the back-scattering geometry commonly used in standard XMCD measurements. This new cavity design illustrated with Fig. 2b) allowed us: (i) to increase quite significantly the detection efficiency; (ii) to set $\mathbf{H}_0$ nearly perpendicular to the YIG film with the advantage that larger precession angles can be reached. In our improved design, the electrical continuity of the cavity walls was preserved using a well polished Be window ($\oslash$ 31 mm; thickness: 25 μm) which makes it also possible to collect the X-ray fluorescence photons over a wider solid angle using a photodiode located very close to the sample and which has a rather large active area (300 mm^2). This photodiode has a 4 mm $\oslash$ hole at its center to let the incident X-ray beam pass through the Si wafer and enter the cavity.

In both configurations, we used PNN^+ Si photodiodes designed in close collaboration with Canberra-Eurisys in order to preserve a very low capacitance: actually, the detector capacitance was found to be ≤ 11 pF for the 80 mm^2 active area photodiode used in configuration a), and ≤ 26 pF for the photodiode used in configuration b). In all cases, the detector was carefully shielded using an ultra-thin Be window which protected us against misleading artefacts due to the unwanted direct detection by the photodiode of leaking microwaves. The detector readout electronics was the same: it included a homemade, magnetically shielded, ultra-low noise preamplifier combined with a multichannel Vector Spectrum Analyzer (Agilent Technologies Inc. VSA 89600-S) exploiting 23-bits digitizers. The dynamic range of the whole detection system was checked to exceed 126 dBc.

EXPERIMENTS

The experiments were performed on a high quality thin film of YIG (8.9 μm thick) grown by liquid phase epitaxy on a (111) GGG substrate. Samples (2x2mm^2) were glued on low loss sapphire rods ($\oslash$ 4mm) terminated by a flat surface making the desired tilt angle with respect to the rod axis: $\beta_N = -30^\circ$ for the old cavity design; $\beta_N = -6^\circ$ for the new cavity design.

Conventional FMR spectra were first measured at low microwave power with our spectrometer: as anticipated, these spectra exhibited a very rich pattern of sharp lines assigned to magnetostatic modes [5]. Unfortunately, the resonance of the uniform mode vanished due to a very high radiation damping effect. The signal of the uniform mode could be nevertheless easily recovered by simply overcoupling the cavity ($Q_L \approx 800$) and off-setting the microwave frequency from F_{cav} by typically 5-10 MHz. In a true perpendicular magnetization geometry, the linewidth of the uniform mode was found to be quite narrow since: $\Delta H_{fwhm}(\beta_N = 0^\circ) = \sqrt{3}\Delta H_{pp} = 1.13$ Oe. However, ΔH_{fwhm} increased to 1.21 Oe for $\beta_N = -6^\circ$;

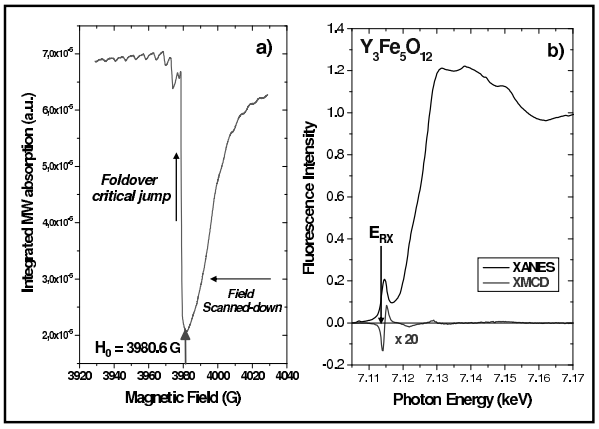

FIGURE 3. XDMR settings: a) resonant pumping near the critical foldover jump; b) XMCD probe.

2.16 Oe for $\beta_N = -16^\circ$ and finally 3.64 Oe for $\beta_N = -30^\circ$. We also measured carefully the linear dependence of the linewidth as a function of the microwave frequency in order to determine the *intrinsic* linewidth from the slope: 0.04 Oe/GHz. This figure may be converted into a Gilbert damping factor of *ca.* 6.0 10^{-5} which confirms the high quality of the YIG film prepared in Brest.

For XDMR experiments, we clearly need to maximize the precession angle θ_0. For a ferromagnetic YIG film magnetized perpendicularly, the maximum precession angle $\theta_{0_{max}}$ at resonance is given by [9]: $\theta_{0_{max}} = h_p/\Delta H_{fwhm}$ in which it is assumed that a *linearly* polarized microwave pump field (h_p) is used. It immediately appears that the choice of YIG films is most propitious due to very narrow linewidths. It remains nevertheless mandatory to increase the microwave power in order to properly scale h_p. In our experiments, the incident microwave power was increased up to 28 dBm: this would correspond typically to $h_p \simeq 0.75$ Oe if one neglects radiation damping corrections. Clearly, resonant pumping occurred then in the non-linear foldover regime in which the lineshapes are heavily distorted. Moreover, it is well documented that, in the foldover regime, $\theta_{0_{max}}$ can never be reached when the microwave power is amplitude modulated [9]: the highest precession angle is obtained at the critical instability resonance field H_{C2} where the slope $d\theta_0/dH_0$ becomes infinite with $\theta_{0_{C2}} \ll \theta_{0_{max}}$. As illustrated with Fig. 3a), the resonance field (H_0) was then carefully scanned down to the onset of the critical foldover jump, *i.e.* at $H_{C2} = 3980.6$ Oe in our first experiment [2]. The energy of the X-ray monochromator was tuned to 7113.74 eV, *i.e.* to the maximum of the XMCD signal in the pre-peak of the XANES spectrum (Fig. 3b).

We found most convenient to carry out our XDMR experiments when the ESRF machine was operated in the 2x1/3 filling mode: this implied that the X-ray beam

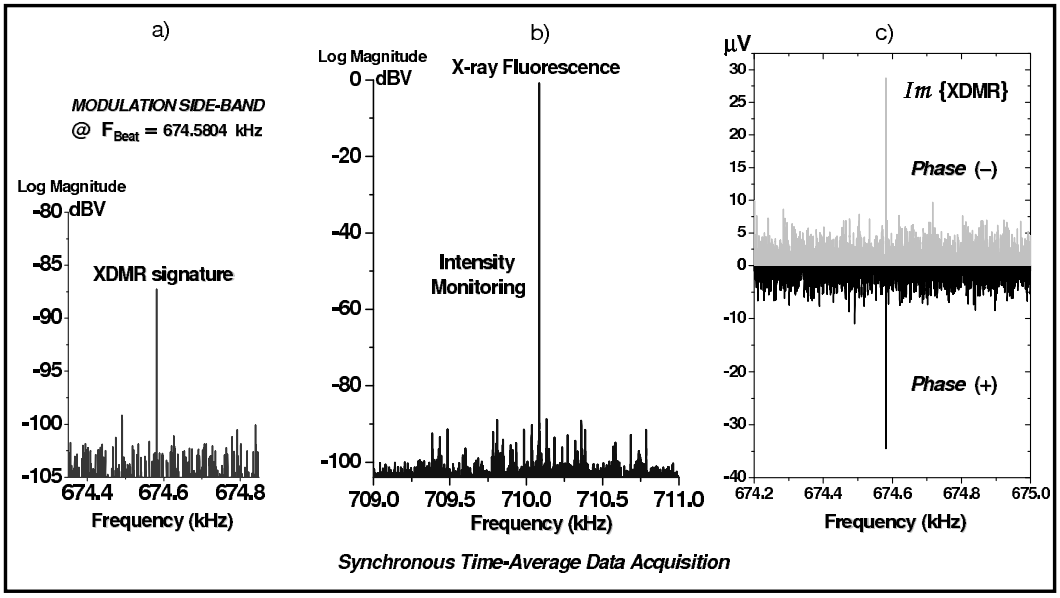

FIGURE 4. a) Low-frequency side-band associated with the XDMR signal; b) X-ray Fluorescence intensity monitoring at $F_{RX} = 2xF_0 = 710.084$ kHz; c) Switching the X-ray helicity from left to right, *i.e* the undulator phase from (+) to (-), is nicely inverting the XDMR signal.

was intrinsically modulated at the macrobunch repetition frequency: $F_{RX} = 2xF_0 = 710.084$ kHz in which $F_0 = RF/992$ is the revolution frequency of the electrons in the storage ring. Indeed, the amplitude modulation of the microwave power had to be rigourously synchronized with the microbunch time-structure. For the experiments reported in reference [2], the microwave power was square modulated at a frequency $F_m = 2xF_0/20 = 35.5042$ kHz triggered from the radiofrequency master clock of the ESRF storage ring. Since the very short rise/fall time of the microwave pulses could cause a very weak -but yet undesirable- contamination of the XDMR signal with high order *odd* harmonics of F_m, we found it much safer to select now a different modulation frequency: $F_m = 2xF_0/25 = 28.4034$ kHz in order to get rid of this problem.

Data acquisition was performed in the synchronous time-average mode of the VSA using an external triggering signal at F_m. The XDMR signature was then expected to appear as modulation sidebands at $F = F_{RX} \pm F_m$. We have reproduced in Fig. 4a) the XDMR signal measured in our first experiment [2]: it appears as expected at $F_1 = 674.58$ kHz and is peaking *ca.* 17 dBV above the noise floor which reflects mostly the contribution of the statistical noise of the X-ray source. The high dynamic range of our detection system is well illustrated with Fig. 4b) which displays the signal measured at F_{RX} that is used only for intensity monitoring /data renormalization. Note that the calculated differential cross-section normalized to the edge jump is quite small: $\Delta\sigma_{XDMR} \approx 1.34\ 10^{-5}$. As shown in Fig. 4c), the XDMR signal, just like XMCD, gets nicely inverted for opposite phases of the helical undulator, *i.e.* when the helicity of the incoming X-ray photons is switched from left to right.

One may check with Fig. 5a) that the cavity design of Fig. 2b) resulted in a major improvement since the XDMR signal recorded at the Fe K-edge is now peaking *ca.* 34 dBV above the noise floor whereas the normalized differential cross-section increased significantly: $\Delta\sigma_{XDMR}(Fe) \approx 3.35\ 10^{-5}$. This is slightly less than what was expected from the reduction of the sample tilt angle ($\beta_N \rightarrow 6^\circ$) because the benefit of a narrower linewidth was partly counter-balanced by a stronger radiation damping effect.

We also succeeded in detecting with this sample a nice XDMR signal at the yttrium L_3-edge: this experiment was most challenging because the flux of the incident X-rays was much lower whereas the fluorescence yield at the Y L-edges is fairly poor. The results are displayed in Fig. 5b): the relevant XDMR signal is peaking *ca.* 24 dBV above a noise floor that is fairly low while there is a marked reduction of the amplitude of the peak at $F_{RX} = 710.084$ kHz monitoring the fluorescence intensity. Recall, however, that the latter raw signal is *not* corrected yet for any pre-edge background intensity (-40 dBV). After proper corrections, the calculated XDMR differential cross-section normalized to the Y L_3 edge jump: $\Delta\sigma_{XDMR}(YL_3) \approx 2.65\ 10^{-4}$ was found larger than the corresponding quantity measured at the Fe K-edge although the latter experiment was a lot easier.

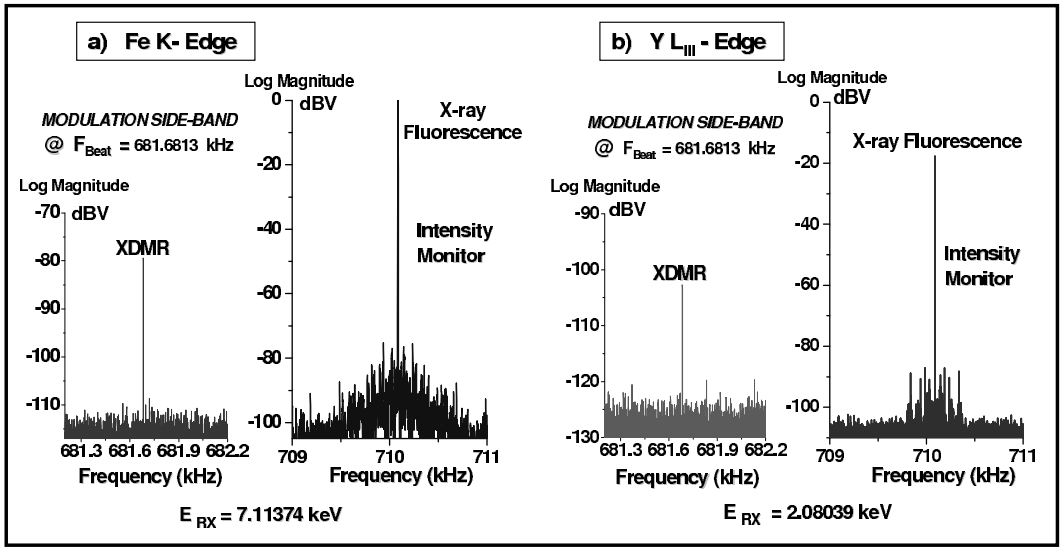

FIGURE 5. XDMR experiments in the backscattering geometry at the Fe K-edge (a) and Y L_3 -edge (b).

DISCUSSION

For a ferromagnetic thin film with true uniaxial anisotropy and near-normal magnetization [9], the precession opening angle is a constant of the motion even in the foldover regime. On combining XDMR with *static* XMCD measurements performed under similar conditions, one may determine quite reliably the opening angle θ_0 of the precessing moments. In the most favourable longitudinal detection geometry ($\mathbf{k}_x = \mathbf{k}_{\|}$), one would show that: $[\Delta\sigma_{XDMR}(k_{\|})]/[\Delta\sigma_{XMCD}(k_{\|})] \simeq -1/2\tan^2\theta_0$ in which the $\Delta\sigma_j$ refer to the relevant differential X-ray absorption cross-sections. Under the conditions of our first experiment (Fig. 4a), our estimate of the precession angle near critical foldover was [2]: $\theta_0 \simeq 3.5^\circ$. Under the conditions of our recent experiment illustrated with Fig. 5a), this precession angle increased up to 5.5°.

Recall that the effective operators responsible for XMCD at a K-edge are purely of *orbital* origin [1]. As discussed elsewhere [2, 9], the effective operator accounting for XMCD at the Fe K-edge could be written: $\frac{d}{dE}[\langle L_z\rangle_{4p} + \varepsilon\langle L_z\rangle_{3d}]$, these two terms reflecting the respective contributions of electric dipole ($E1$) and electric quadrupole ($E2$) transitions. Our XDMR experiments at the Fe K-edge produce therefore a direct evidence of the forced precession of orbital magnetization DOS. In this respect, XDMR appears as a unique and very promising tool to investigate the precession dynamics of orbital magnetization components [9].

In contrast, one would check from a direct use of the XMCD sum rules, that the magnetization components induced at the *"non-magnetic"* yttrium sites are essentially of spin origin. Moreover, the induced moments are antiferromagnetically coupled to the Fe spins through superexchange *via* the oxygen lattice. The precession angle deduced from our Y L_3-edge XDMR measurements (*ca.* 6.6°) is only slightly larger than the precession angle measured under strictly the same conditions at the Fe K-edge (5.5°). The implications of this interesting result will be discussed elsewhere.

ACKNOWLEDGMENTS

Technical assistance by S. Feite and P. Voisin is warmly acknowledged. The authors very much appreciated the constant support of Y. Petroff and of the successive ESRF Directors given to this project.

REFERENCES

1. A. Rogalev *et al.* "X-ray Magnetic Circular Dichroism", in *Magnetism: A Synchrotron Radiation Approach*, edited by E. Beaurepaire *et al.*, *Lectures Notes in Physics* **697**, Berlin: Springer Verlag, 2006, pp. 71–94.
2. J. Goulon *et al.*, *JETP Letters* **82**, 791-796 (2005).
3. K. Gnatzig *et al.*, *J. Appl. Phys.* **62**, 4839–4843 (1987).
4. W.E. Bailey *et al.*, *Phys. Rev. B* **70**, 172403 (2004).
5. A. G. Gurevich, G. A. Melkov "Magnetization Oscillations and Waves", Boca Raton: CRC Press Inc., 1996.
6. N. Bloembergen, S. Wang, *Phys. Rev.* **93**, 72-83 (1954).
7. J. Goulon *et al.*, *J. Synchrotron Rad.* **5**, 232-38 (1998).
8. J. Goulon *et al.*, *Proc. of the 9th Internat. Conf. on* "Synchrotron Radiation Instrumentation" (SRI-2006), Daegu/Korea (2007).
9. J. Goulon *et al.*, *Eur. Phys. J. B, accepted for publication*.